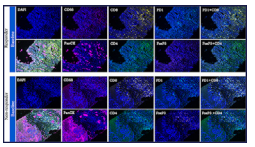

Immune Modulation in Untreated, Contralateral Hepatic Metastases after Yttrium-90 Radioembolization of Microsatellite Stable Colorectal Cancer

Elif Öcal, MD, Marianna Alunni-Fabbroni, PhD, Ignazio Piseddu, MD, Matthias Thaler, MD, Mathias J. Zacherl, MD, Lukas Salvermoser, MD, Matthias M.R. Stechele, MD, Lu Fornés Burnell, Heidrun Hirner-Eppeneder, PhD, Melanie A. Kimm, PhD, Martina Rudelius, MD, Max Seidensticker, MD, Moritz Wildgruber, MD, S. Nahum Goldberg, MD, and Jens Ricke, MD

ABSTRACT

Purpose: To assess immunogenic effects in unembolized contralateral tumor after single lobar yttrium-90 transarterial radioembolization (^{90}Y-TARE) of colorectal liver metastases (CRLMs).

Material and Methods: The analysis comprised 10 patients with microsatellite stable (MSS) CRLM scheduled for staged treatment in the prospective AROMA trial. Eligibility criteria included bilobar metastatic disease with >5 lesions without any treatment within 3 weeks. Baseline biopsy was followed by initial ^{90}Y-TARE treatment of 1 liver lobe, followed by a second biopsy of yet untreated tumors in the other liver lobe at a median of 13 days (range, 4–49 days) immediately before second treatment. Tumor biopsies and peripheral blood mononuclear cells (PBMCs) were collected before treatments for immune cell analysis. Patients were stratified into responders and nonresponders based on tumor control or progression during follow-up.

Results: At baseline, responders (n = 4) displayed lower concentrations of FoxP3$^+$ cells and colocation of CD4$^+$FoxP3$^+$ cells than nonresponders (both P = .02) in tumor tissues. At second biopsy, nonresponders showed a higher CD68$^+$ macrophage density (P = .0014) than responders. Responders displayed fewer CD4$^+$FoxP3$^+$ T cells than CD8$^+$ T cells at all time points (P = .02 and P = .0428). Nonresponders demonstrated a trending increase in CD68$^+$ macrophages (P = .062), as well as a higher CD8$^+$PD1$^+$/CD8$^+$ ratio (P = .062). PBMCs of nonresponders displayed lower CD8$^+$PD1$^+$ T cells and CD8$^+$PD1$^+$/CD8$^+$ ratio at both time points.

Conclusions: ^{90}Y-TARE induces local immunogenic effects in nonexposed MSS CRLM, as well as systemic exhaustion of immune cells in nonresponders. Clinical implications such as a prognostic role or synergism of ^{90}Y-TARE and checkpoint inhibition in MSS CRLM warrant further investigation.

ABBREVIATIONS

CRC = colorectal cancer, CT = computed tomography, IHC = immunohistochemistry, MMR = mismatch repair, MR = magnetic resonance, MSS = microsatellite stable, ^{90}Y = yttrium-90, PBMC = peripheral blood mononuclear cell, ROI = region of interest, TARE = transarterial radioembolization

Colorectal cancer (CRC) is the third most common malignant tumor and the second most common cause of cancer-related death, with an estimated 881,000 deaths recorded worldwide in 2018 (1). Unlike many other gastrointestinal tumors, response to checkpoint inhibition in CRC is limited to patients with mismatch repair (MMR) deficiency, which accounts only for up to 15% of cases (2,3). Yttrium-90 transarterial radioembolization (^{90}Y-

Appendix A, **Figures E1** and **E2**, and **Tables E1–E4** can be found by accessing the online version of this article on *www.jvir.org* and selecting the Supplemental Material tab.

J Vasc Interv Radiol 2024; 35:1793–1805
https://doi.org/10.1016/j.jvir.2024.07.010

RESEARCH HIGHLIGHTS

- Microsatellite stable colorectal cancer has not demonstrated favorable outcomes with immunotherapeutic approaches including checkpoint inhibition. Radioembolization has indicated potential as an immunomodulator.
- Yttrium-90 radioembolization induced nontarget immune effects in patients with microsatellite stable colorectal cancer.
- Immune expression status after radioembolization correlated with patient outcome.

TARE) is an established locoregional treatment option for patients with CRC advanced liver metastases (4). In other gastrointestinal tumors such as hepatocellular carcinoma, ^{90}Y-TARE has demonstrated immunogenic effects leading to improved patient outcomes (5). The underlying mechanisms supporting immunomodulation by ^{90}Y-TARE are unknown, as well as the potential for synergism with combined checkpoint inhibition. Two previous studies in patients with advanced CRC liver metastases demonstrated no benefit of combining ^{90}Y-TARE with checkpoint inhibition as both reported an overall response rate of 0% (6,7). One of these studies (6) added tissue specimen from selected patients showing no immune cell infiltration in liver metastatic tumor, which, in contrast to the study presented herein, had been exposed to radioembolization.

Nevertheless, distant effects following ^{90}Y-TARE of liver metastases leading to a measurable response in untreated tumors have been described previously with low prevalence (8). This study, using patients with MSS liver metastases undergoing ^{90}Y-TARE, sought to describe immunogenic effects in nontarget liver metastases at a cellular level by (*a*) phenotypically characterizing the cellular subsets that enrich the tumor microenvironment after ^{90}Y-TARE, (*b*) evaluating the expression of programmed cell death (PD) 1 in response to ^{90}Y-TARE, (*c*) examining the immune profiles of the peripheral blood mononuclear cells (PBMCs) longitudinally in a subset of patients, and (*d*) identifying cellular markers that may predict therapy response after ^{90}Y-TARE.

MATERIALS AND METHODS

Ethical Consideration

This study represents a subanalysis of the AROMA trial (German Clinical Trials Register-ID: DRKS00009744). The study has been approved by the institutional ethical board (protocol number 17-290). Study conduct was in accordance with the Declaration of Helsinki. Before entering the study, all patients were fully informed by the treating physician of the scope and goals of the trial, had given written informed consent, and were willing to comply with the study protocol.

STUDY DETAILS

Study type: Prospective, observational, descriptive study

Study phase: NA

Level of evidence: 3 (SIR-C)

Study Design

The AROMA trial had primarily been designed to detect immune signals after ^{90}Y radioembolization on a cellular level in tumor tissue and blood, recruiting patients of various tumor entities. The subanalysis described herein included all available patients with MSS colorectal liver metastasis. At study inclusion, all patients exhibited bilobar liver metastatic disease, and the multidisciplinary team had opted for staged treatment of each liver lobe (9,10). Histological confirmation by percutaneous biopsy of liver lesions was performed at baseline. All patients then underwent unilobar ^{90}Y-TARE. ^{90}Y-TARE, including preprocedural diagnostic workup, was performed according to a standard algorithm as described previously using ^{90}Y resin microspheres (SIR-Spheres; Sirtex Medical, Woburn, Massachusetts) (11). The workup included technetium-99m macroaggregated albumin planar imaging to estimate the lung shunt fraction and single-photon emission computed tomography (CT)/CT imaging to exclude extrahepatic accumulations. Body surface area method was used for dose calculation. After a median of 13 days (range, 4–49 days), patients were scheduled for the second contralateral treatment, which, according to study protocol, could be performed by local ablation (if technically feasible) and include a biopsy of the target lesion. Thereby and with ethics approval, all patients underwent a second biopsy of yet untreated tumor in the contralateral liver lobe. Tissue acquisition preceded the preplanned local ablation of these therapy-naïve tumors. As a result, biopsied tissues from therapy-naïve tumors were collected before ^{90}Y-TARE (baseline) and immediately before a prescheduled, subsequent ablation procedure (time point 2). Tissue samples were obtained through an 18-gauge coaxial biopsy needle, fixed in 10% formalin overnight at 4°C, and subsequently embedded in paraffin. Five out of 10 patients underwent biopsy of identical tumors at baseline and at time point 2.

Follow-up and Definition of Response

Clinical visits were scheduled every 6 weeks after second intervention. Clinical follow-up included contrast-enhanced thorax/abdomen CT and hepatobiliary magnetic resonance (MR) imaging at baseline, 6 weeks after completion of the second intervention, and every 3 months after second intervention. Patients were stratified as responders and nonresponders. Responders were defined by objective response (partial/complete response) or stable disease at 6 months according to Response Evaluation Criteria in Solid Tumors 1.1. (RECIST 1.1.). Assessments included target and nontarget lesions, as well as any other tumor progression.

Table 1. Baseline Characteristics of the Study Population (n = 10)

Baseline characteristics	N = 10 (% or range)	Responder	Nonresponder	*P*
Age (mean ± SD)	62.8 ± 11.8	68 ± 9.5	59.3 ± 12.7	.14
Sex (male/female)	9 (90.0)/1 (10.0)	3 (75.0)/1 (25.0)	6 (100)/0 (0)	.40
CEA				
<200 ng/mL	4 (40)	1 (25)	3 (50)	.57
>200 ng/mL	6 (60)	3 (75)	3 (50)	
KRAS mutation				
Wild	2 (20)	2 (50)	0 (0)	.33
Mutant	6 (60)	2 (50)	4 (66)	
Unknown	2 (20)	0 (0)	2 (33)	
Mismatch repair deficiency: MSS	10 (100)*			
Primary lesion site				
Right hemicolon	2 (20)	1 (25)	1 (66)	.71
Left hemicolon	5 (50)	1 (25)	4 (16)	
Rectum	3 (30)	2 (50)	1 (16)	
Primary tumor N staging				
N0	3 (30)	1 (25)	2 (33)	>.99
$N1^+$	7 (70)	3 (75)	4 (66)	
Histologic type				
Adenocarcinoma	9 (90)	3 (75)	6 (100)	.40
Mucinous	1 (10)	1 (25)	0 (0)	
Extrahepatic metastasis				
Yes (pulmoner)	4 (40)	3 (75)	1 (16)	.19
No	6 (60)	1 (25)	5 (83)	
Primary tumor resection				
Yes	6 (60)	3 (75)	3 (50)	>.99
No	4 (40)	1 (25)	3 (50)	
Type of liver metastasis				
Metachronous	4 (40)	2 (50)	2 (33)	>.99
Synchronous	6 (60)	2 (50)	4 (66)	
Pretreatments	1 (10)	1 (25)	0 (0)	.67
None first line	2 (20)	1 (25)	1 (16)	
≥2 lines of systemic therapy	7 (70)	2 (50)	5 (83)	
Best response before inclusion				
PD	2 (20)	1 (25)	1 (16)	.50
SD	3 (30)	0 (0)	3 (50)	
PR	4 (40)	2 (50)	2 (33)	
NA	1 (10)	1 (25)	0 (0)	
ECOG score				
0	5 (50)	2 (50)	3 (50)	>.99
1	5 (50)	2 (50)	3 (50)	
Largest tumor size (mean ± SD)	55.7 ± 28	53.5 ± 28.54	57.16 ± 30.27	.85

CEA = carcinoembryonic antigen; MSS = microsatellite stable; NA = not applicable (therapy naïve); ECOG = Eastern Cooperative Oncology Group; KRAS = Kirsten rat sarcoma virus; PD = progressive disease; PR = partial response; SD = stable disease.
*One patient displayed loss of MSH6 but not MSH2, MLH1, and PMS2 (12).

Study Population

Ten patients with colorectal liver metastases were included (**Fig E1**, available online on the article's Supplemental Material page at *www.jvir.org*). Baseline characteristics are given in **Table 1** (12). Nine patients were male, and the median age was 63.5 years (range, 41–82 years). Nine out of 10 patients had undergone systemic chemotherapy before study inclusion (**Table E1**, available online at *www.jvir.org*). The washout time between last systemic treatment and baseline biopsy was 3 weeks at minimum (median, 59 days; range, 21–522 days). No patient received systemic treatment between baseline and second biopsies. All patients had bilobar metastatic disease with multiple (>5) lesions. Six patients presented Kirsten rat sarcoma virus mutations. All patients were microsatellite stable (MSS) at immunohistochemistry (IHC) screening.

IHC Staining of MMR Proteins

IHC evaluation of MMR protein expression was performed on all tissue sections collected at baseline and time point 2 to confirm the MSS status. Serial tissue sections of 2 µm were cut from formalin-fixed, paraffin-embedded tumor

tissues, dewaxed, and rehydrated according to standard procedure (preheating at 60°C; deparaffinization in Neo-Clear; Merck, Darmstadt, Germany; rehydration in graded series of ethanol and distilled water). For IHC, the primary antibodies anti-MLH1 (dilution 1:100), MSH2 (dilution 1:500), MSH6 (dilution 1:500), and PMS2 (dilution 1:100; Mismatch Repair Antibody Panel; Abcam, Berlin, Germany) were applied overnight at 4°C, followed by incubation with the secondary antibody (goat antirabbit IgG H&L/HRP, dilution 1:2000; Abcam). DAB substrate kit (Cell Signaling Technology, Leiden, Netherlands) was used as the chromogen. Sections were counterstained with Haemalaun (Merck), dehydrated, and mounted using Neo-Mount (Merck). Evaluation of the MMR protein expression status was performed by a board-certified pathologist (E.Ö.). Cases with a complete absence of nuclear staining and positive nuclear staining in internal control cells were considered to demonstrate MMR protein loss.

Multiplex Immunofluorescence Staining

Immunofluorescence of paraffin sections was performed using the Opal 7 Solid Tumor Immunology Kit (Akoya Biosciences; Marlborough, Massachusetts) for the detection of $CD4^+$, $CD8^+$, $FoxP3^+$, $PD1^+$, $CD68^+$, and Pan CK^+ cells according to the protocol's supplier (**Appendix A**, available online at *www.jvir.org*). Individual counts of $CD8^+PD1^+$ and $CD4^+FoxP3^+$ coimmunopositive T cells as well as $CD68^+$ macrophages were obtained (**Table E2**, available online at *www.jvir.org*). For image acquisition and multispectral imaging, Vectra Polaris (Perkin Elmer, Hopkinton, Massachusetts) was used. Positive cells were quantified by analyzing 3 regions of interest (ROIs) of 931 × 698 μm.

PBMC Isolation and Flow Cytometry Analysis

PBMCs were isolated from whole blood collected before therapy (baseline) and at 2 consecutive posttherapy time points (24 hours after ^{90}Y-TARE and time point 2) from 2 responders and 4 nonresponders. PBMCs were isolated by conventional Ficoll-Paque density gradient (Cytiva, Uppsala, Sweden) according to the manufacturer's instruction and preserved in fetal calf serum/10% dimethylsulfoxide at −150°C until analyzed.

For performing fluorescence-activated cell sorting, PBMCs were thawed and rested in RPMI 1640 medium containing 10% fetal calf serum, 1% penicillin/streptomycin, and 1% L-glutamine for 1 hour. Before antibody staining, cells were incubated with Human TruStain FcX (BioLegend, San Diego, California). Extracellular staining was performed with a 1:200 dilution of the respective isotype antibodies and eBioscience Fixable Viability Dye eFluor 780 (ThermoFisher Scientific, Waltham, Massachusetts). Upon permeabilization and fixation of cells with eBioscience Foxp3/Transcription Factor Staining Buffer Set (ThermoFisher Scientific), cells were intracellularly stained with 1:100 diluted antibodies. Stained PBMCs were measured on a BD LSRFortessa Cell Analyzer (BD Biosciences, San Jose, California), and data were subsequently analyzed using FlowJo 10.8.1 (BD BioSciences). The following staining antibodies were used: anti-TIGIT-BV421 (A15153G), anti-CD8-BV510 (SK1), anti-TIM-3-BV650 (F38-2E2), anti-CTLA4-BV711 (BNI3), anti-CD4-PerCP-Cy5.5 (SK3 or RPA-T4), anti-FoxP3-PE (259D), anti-PD-1-PE/Dazzle594 (EH12.2H7), anti-GrzB-PE-Cy7 (QA16A02), anti-CD25-APC (M-T271), and anti-CD3-AF700 (OKT3) (all from Biolegend), as well as Fixable Viability Dye eFluor 780 (ThermoFischer Scientific).

Statistical Analysis

All statistical analyses were performed using SAS version 9.4 for Windows (Copyright SAS Institute, Cary, North Carolina) and GraphPad Prism (version 9; GraphPad Software, San Diego, California). Normality distribution was measured using the Shapiro-Wilk test. Numerical data are presented as means with SDs. For categorical data, results are given as absolute numbers with percentages. For comparison of categorical data, Fisher's exact tests were applied. T-tests or Mann-Whitney U tests were used for testing homogeneity of independent samples in continuous data. Fluorescence-activated cell sorting data are presented as mean with SEM. Statistical comparison between responders and nonresponders are performed using 2-way analysis of variance with Sidak's correction for multiple testing. Statistical analysis of longitudinal values within each response group employed 2-way analysis of variance with Dunnet's correction. Spearman correlation analysis was used to evaulate the correlation between radiation dose and immune response. Wilcoxon 2-sample test was used to analyze a difference in median radiation dose between patients with objective response and patients with no response. Due to the low sample size, no alpha adjustment was made. All statistical tests were interpreted at a signifcance level of $\alpha = 5\%$ with the according results considered exploratory.

RESULTS

Clinical Outcome

No patient experienced treatment-related adverse events. Median overall survival was 8.7 months. According to response assessment, 4 patients were classified as responders and 6 as nonresponders. All ablated lesions displayed local tumor control during follow-up.

Immunophenotyping Characterization of Immune Cells in ^{90}Y-Naïve Tumor Tissue at Time Point 2

First, the distribution of a representative range of immune cells in tumor tissue of responders and nonresponders was investigated separately at baseline and second biopsy (**Fig 1**). At baseline, tumor of responders displayed a lower

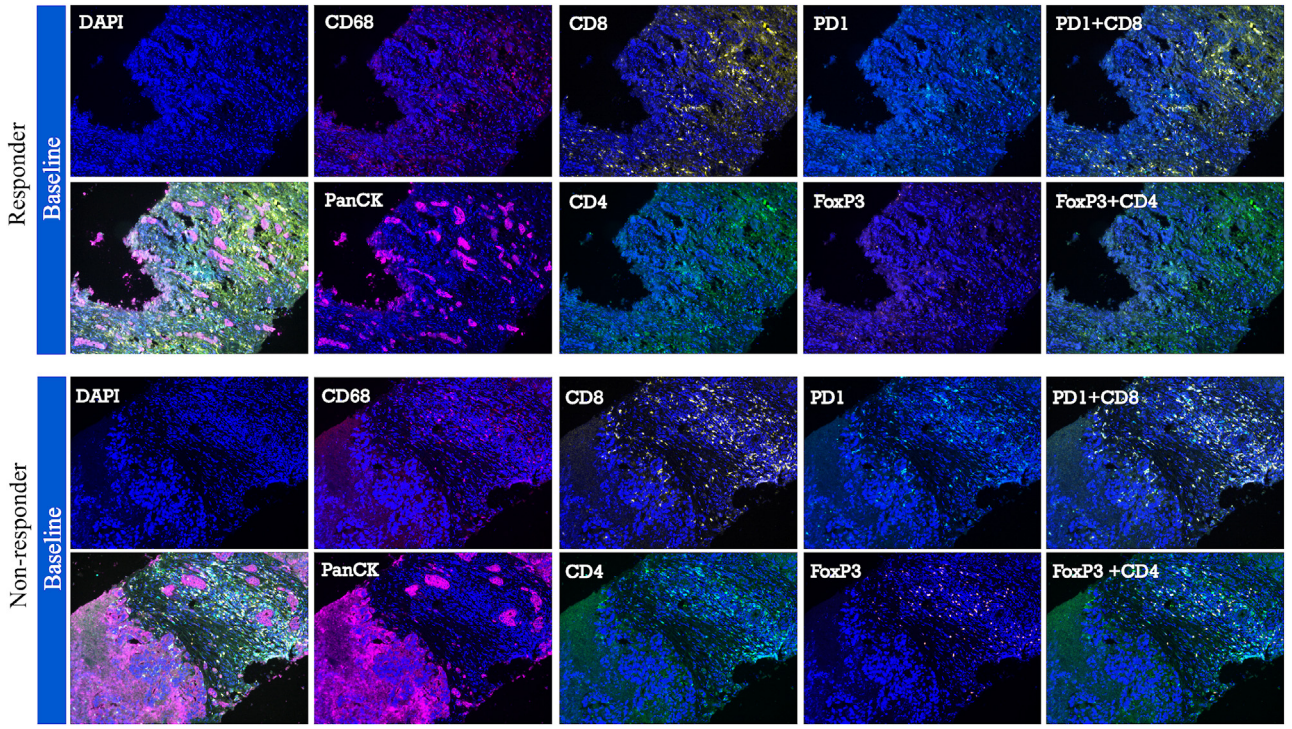

Figure 1. Representative multiplex immunofluorescence images of yttrium-90–naïve tumor tissue of colorectal cancer liver metastasis from a responder and a nonresponder at baseline and time point 2. CD68 (Opal 650, red), CD8 (Opal 570, yellow), PD1 (Opal 540, cyan), cytokeratin (Opal 690 magenta, CD4 (Opal 520, green), FoxP3 (Opal 620, orange), and DAPI (blue). Magnification, ×200. Responders showed a lower amount of FoxP3 and colocalization of CD4 and Foxp3 compared with nonresponders. For image acquisition and multispectral imaging, Vectra Polaris imaging system (Perkin Elmer, Hopkinton, Massachusetts) was used. The size of each region of interest was 931 × 698 μm.

concentration of $FoxP3^+$ regulatory cells (19.25 [SD ± 3.30] vs 67.80 [SD ± 46.77]; $P = .020$) and colocation of $CD4^+FoxP3^+$ T cells (12.25 [SD ± 3.77] vs 47.60 [SD ± 31.42]; $P = .020$) compared with that of nonresponders. No difference was observed in any other immune cell population when comparing responders with nonresponders. At time point 2, nonresponders showed a higher $CD68^+$ macrophages density compared with responders (235.5 [SD ± 61.6] vs 80.6 [SD ± 19.8]; $P = .001$). The statistical analysis of the density of immune cells in ^{90}Y-naïve tumor tissue of responders and nonresponders is outlined in Table 2.

Relative ratios of $CD4^+FoxP3^+$, $CD8^+$, and $CD8^+PD1^+$ T Cells in ^{90}Y-Naïve Tumor Tissue at Time Point 2

Responders displayed a lower $CD4^+FoxP3^+/CD8^+$ cells ratio (Fig 2a) when comparing the amount of $CD4^+FoxP3^+$ regulatory T cells with the amount of $CD8^+$ cytotoxic T cells in the same ROI. This finding was independent of the time point. By comparing density of $CD8^+PD1^+$ T cells with $CD8^+$T cells in the same ROI, a lower $CD8^+PD1^+/CD8^+$ T cell ratio at time point 2 (after distant ^{90}Y exposure) but not at baseline was found and associated with response (Fig 2b). The statistical analysis of immune cell ratios in ^{90}Y-naïve tumor tissue of responders and nonresponders is shown in Table 3.

Changes in Immune Cell Infiltration from Baseline to Time Point 2

Further, changes in density of different immune types in tumor tissue at baseline versus time point 2 in responders and nonresponders were assessed (Fig 3). $CD8^+$ T-cell density showed a decrease in untreated tumor tissue of nonresponders after distant ^{90}Y-TARE, with the ratio between time point 2 $CD8^+$ T cell and baseline $CD8^+$ T cells ranging from 0.18 to 0.65 ($P = .062$); however, because of the lower sample size, it could not reach statistical significance (Table E3, available online at *www.jvir.org*). In nonresponders, $CD68^+$ macrophages showed an increased density at time point 2, with a ratio between 1.24 and 2.52 ($P = .062$); however, because of the lower sample size, it could not reach statistical significance (Table E3). A trend to higher $CD8^+PD1^+/CD8^+$ ratio was observed at time point 2 with a ratio between 1.14 and 10.73; however, because of the lower sample size, it could not reach statistical significance ($P = .062$) (Table E3).

Table 2. Descriptive Statistics of Immune Cells Identified in Yttrium-90–Naïve Tumor Tissue

Parameter	Statistics	Total	Groups		*P*
			Responder	Nonresponder	
$CD4^+$ baseline	*P*				.066
	n/n_{miss}	9/1	4/0	5/1	
	Mean (SD)	198.33 (94.12)	135.25 (56.30)	248.80 (90.43)	
	95% CI	125.98–270.68	45.66–224.84	136.52–361.08	
	Median (IQR)	190.00 (119.00)	137.00 (93.50)	255.00 (104.00)	
	Minimum–maximum	73.00–369.00	73.00–194.00	136.00–369.00	
$CD4^+$ time point 2	*P*				.676
	n/n_{miss}	10/0	4/0	6/0	
	Mean (SD)	144.00 (65.31)	132.50 (40.71)	151.67 (80.66)	
	95% CI	97.28–190.72	67.71–197.29	67.02–236.31	
	Median (IQR)	140.00 (53.00)	133.50 (60.00)	143.50 (53.00)	
	Minimum–maximum	58.00–298.00	83.00–180.00	58.00–298.00	
$FoxP3^+$ baseline	*P*				**.020**
	n/n_{miss}	9/1	4/0	5/1	
	Mean (SD)	46.22 (41.87)	19.25 (3.30)	67.80 (46.77)	
	95% CI	14.04–78.40	13.99–24.51	9.72–125.88	
	Median (IQR)	26.00 (34.00)	19.00 (5.50)	55.00 (23.00)	
	Minimum–maximum	16.00–147.00	16.00–23.00	26.00–147.00	
$FoxP3^+$ time point 2	*P*				.649
	n/n_{miss}	10/0	4/0	6/0	
	Mean (SD)	31.60 (22.72)	27.25 (18.79)	34.50 (26.30)	
	95% CI	15.35–47.85	–2.64 to 57.14	6.90–62.10	
	Median (IQR)	29.50 (28.00)	31.00 (30.50)	28.50 (28.00)	
	Minimum–maximum	4.00–81.00	4.00–43.00	11.00–81.00	
$CD4^+FoxP3^+$ baseline	*P*				**.020**
	n/n_{miss}	9/1	4/0	5/1	
	Mean (SD)	31.89 (29.09)	12.25 (3.77)	47.60 (31.42)	
	95% CI	9.53–54.25	6.24–18.26	8.59–86.61	
	Median (IQR)	24.00 (20.00)	12.00 (5.50)	33.00 (30.00)	
	Minimum–maximum	8.00–99.00	8.00–17.00	24.00–99.00	
$CD4^+FoxP3^+$ time point 2	*P*				.236
	n/n_{miss}	10/0	4/0	6/0	
	Mean (SD)	20.90 (18.05)	12.25 (6.18)	26.67 (21.54)	
	95% CI	7.99–33.81	2.41–22.09	4.06–49.27	
	Median (IQR)	15.00 (16.00)	15.00 (6.50)	20.00 (25.00)	
	Minimum–maximum	3.00–64.00	3.00–16.00	7.00–64.00	
$CD8^+$ baseline	*P*				.459
	n/n_{miss}	9/1	4/0	5/1	
	Mean (SD)	174.44 (88.35)	148.00 (53.60)	195.60 (110.44)	
	95% CI	106.53–242.35	62.71–233.29	58.47–332.73	
	Median (IQR)	156.00 (95.00)	153.50 (89.00)	156.00 (155.00)	
	Minimum–maximum	86.00–357.00	86.00–199.00	102.00–357.00	
$CD8^+$ time point 2	*P*				.594
	n/n_{miss}	10/0	4/0	6/0	
	Mean (SD)	153.80 (154.92)	222.25 (226.61)	108.17 (78.37)	
	95% CI	42.98–264.62	–138.34 to 582.84	25.93–190.41	
	Median (IQR)	108.00 (176.00)	162.00 (322.50)	94.50 (101.00)	
	Minimum–maximum	19.00–538.00	27.00–538.00	19.00–234.00	
$PD1^+$ baseline	*P*				.174
	n/n_{miss}	9/1	4/0	5/1	
	Mean (SD)	52.56 (45.17)	29.75 (11.70)	70.80 (55.16)	
	95% CI	17.83–87.28	11.13–48.37	2.31–139.29	
	Median (IQR)	47.00 (27.00)	25.00 (14.50)	50.00 (53.00)	
	Minimum–maximum	4.00–147.00	22.00–47.00	4.00–147.00	

continued

Table 2. Descriptive Statistics of Immune Cells Identified in Yttrium-90–Naïve Tumor Tissue *(continued)*

Parameter	Statistics	Total	Groups		*P*
			Responder	Nonresponder	
$PD1^+$ time point 2	*P*				.392
	n/n_{miss}	10/0	4/0	6/0	
	Mean (SD)	49.20 (42.81)	40.00 (48.36)	55.33 (42.23)	
	95% CI	18.57–79.83	−36.95 to 116.95	11.02–99.65	
	Median (IQR)	34.00 (91.00)	23.00 (64.00)	39.50 (80.00)	
	Minimum–maximum	4.00–112.00	4.00–110.00	13.00–112.00	
$CD8^+PD1^+$ baseline	*P*				.178
	n/n_{miss}	9/1	4/0	5/1	
	Mean (SD)	28.78 (32.46)	12.25 (7.41)	42.00 (39.67)	
	95% CI	3.83–53.73	0.46–24.04	−7.26 to 91.26	
	Median (IQR)	19.00 (16.00)	13.00 (12.50)	24.00 (38.00)	
	Minimum–maximum	3.00–103.00	4.00–19.00	3.00–103.00	
$CD8^+PD1^+$ time point 2	*P*				.241
	n/n_{miss}	10/0	4/0	6/0	
	Mean (SD)	23.50 (24.47)	10.00 (8.83)	32.50 (28.07)	
	95% CI	6.00–41.00	−4.05 to 24.05	3.04–61.96	
	Median (IQR)	17.00 (15.00)	8.50 (12.00)	19.50 (40.00)	
	Minimum–maximum	1.00–78.00	1.00–22.00	6.00–78.00	
$CD68^+$ baseline	*P*				.472
	n/n_{miss}	9/1	4/0	5/1	
	Mean (SD)	152.56 (36.28)	142.00 (44.62)	161.00 (30.63)	
	95% CI	124.67–180.44	70.99–213.01	122.96–199.04	
	Median (IQR)	162.00 (31.00)	151.00 (63.00)	169.00 (11.00)	
	Minimum–maximum	81.00–194.00	81.00–185.00	111.00–194.00	
$CD68^+$ time point 2	*P*				**.001**
	n/n_{miss}	10/0	4/0	6/0	
	Mean (SD)	173.60 (92.89)	80.75 (19.81)	235.50 (61.65)	
	95% CI	107.15–240.05	49.24–112.26	170.80–300.20	
	Median (IQR)	170.50 (152.00)	87.00 (24.50)	239.00 (75.00)	
	Minimum–maximum	52.00–314.00	52.00–97.00	136.00–314.00	

CI = confidence interval; IQR = interquartile range.
Bold indicates statistical significance.

Immune Cell Infiltration in Tumor versus Adjacent Liver Tissue at Time Point 2

Distribution of immune cells in liver parenchyma versus tumor at time point 2 was assessed in a responder and nonresponder. Enrichment of immune cells was limited to the tumor microenvironment in all samples (**Fig E2**, available online at *www.jvir.org*).

Changes in Peripheral Blood Lymphocytes in Response to ^{90}Y-TARE

To assess whether immunogenic response to ^{90}Y-TARE in tumor tissue was accompanied by systemic immune effects, flow cytometry of PBMC was added. Longitudinal peripheral blood samples were used at baseline, 24 hours after ^{90}Y-TARE, and at time point 2 in a subgroup of patients (responders, n = 2; nonresponders, n = 4). Nonresponders showed a trend to higher percentage of $CD4^+$ T cells compared with responders at time point 2 ($P = .066$). A significant decrease of $CD8^+$ T cells ($P = .033$) in responders and a trend of decreasing $CD4^+CD25^+FoxP3^+$ T cells ($P = .056$) in nonresponders (**Fig 4a**) was observed. Next, different exhaustion markers (PD1, TIGIT, TIM-3, and CTLA4) were investigated on $CD8^+$ T cells at 3 time points (**Fig 4b**; **Table E4**, available online at *www.jvir.org*). A lower percentage of $CD8^+PD1^+$ T cells was observed in nonresponders at baseline ($P = .044$) and at time point 2 ($P < .001$) compared with that in responders. In nonresponders, a significantly lower percentage of posttherapy $CD8^+$ T cells expressed exhaustion marker TIGIT alone or in combination with PD1 ($P = .004$ and $P = .035$, respectively). Next, to evaluate if the killing capacity of $CD8^+$ T cells was altered after therapy, the amount of cytotoxic T cells positive for granzyme B was measured (**Fig 4c**). In responders, a trend to significant increase was observed in the percentage of $CD8^+GzmB^+$ T cells at time point 2 ($P = .064$). A decrease in posttherapy $CD8^+$ T cells expressing granzyme B in nonresponders as well as their lower level in responders failed proving significance ($P = .065$ and $P = .486$, respectively). Finally, the comparison between responders and nonresponders revealed that nonresponders had a

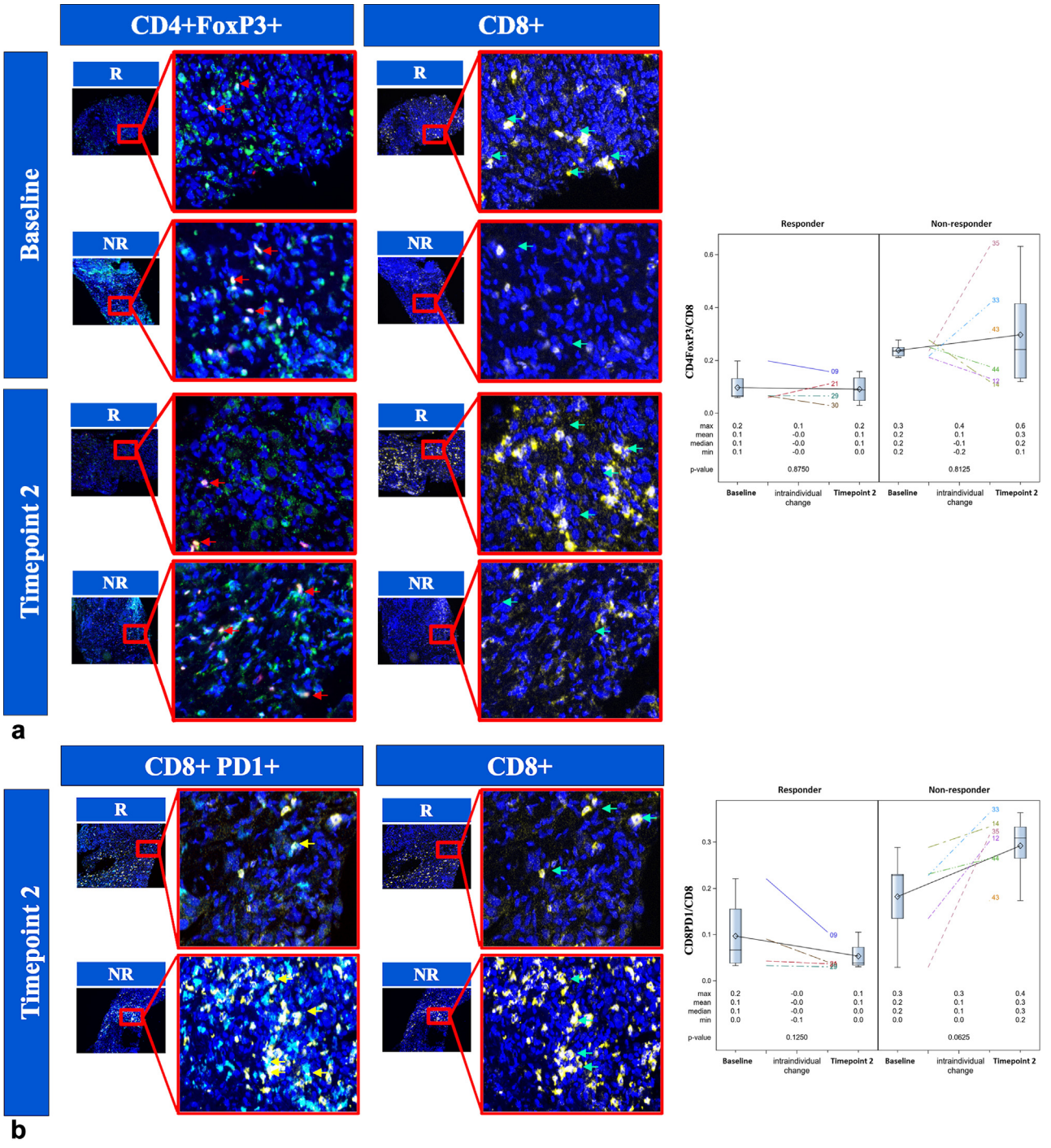

Figure 2. Representative images showing colocalization of tumor infiltrating lymphocytes in tumor tissue of responders and nonresponders at baseline and time point 2. **(a)** A consistently decreasing number of $CD4^+FoxP3^+$ cells and a greater amount of $CD8^+$ cells were found in responders at both time points, whereas a higher amount of $CD4^+FoxP3^+$ cells and a lower amount of $CD8^+$ cells were observed in nonresponders at both time points. **(b)** Responders had lower amounts of $CD8^+PD1^+$ cells and a higher amount of $CD8^+$ cells at time point 2 only. Green, CD4 staining; orange, FoxP3; and yellow, CD8; cyan, PD1 staining; red arrows, colocalization of CD4 and FoxP3; green arrows, CD8 T cells; and purple arrows, colocalization of $CD8^+PD1^+$ on T cells. The size of each region of interest is 931 × 698 μm.

lower (or trending to a lower) $CD8^+PD1^+/CD8^+$ ratio at all time points (baseline, $P = .045$; 24 hours after ^{90}Y-TARE, $P = .080$; time point 2, $P < .001$). No significant difference between the patient groups was found with respect to $CD4^+CD25^+FoxP3/CD8^+$ ratio at any time point (Fig 4d).

Table 3. Descriptive Statistics of Immune Cell Ratio in Yttrium-90–Naïve Tumor Tissue

Parameter	Statistics	Total	Groups		*P*
			Responder	Nonresponder	
$CD4^+FoxP3^+/CD4^+$ baseline	*P*				.071
	n/n_{miss}	9/1	4/0	5/1	
	Mean (SD)	0.15 (0.07)	0.10 (0.05)	0.18 (0.06)	
	95% CI	0.09–0.20	0.03–0.17	0.10–0.26	
	Median (IQR)	0.13 (0.08)	0.09 (0.07)	0.19 (0.09)	
	Minimum–maximum	0.06–0.27	0.06–0.16	0.11–0.27	
$CD4^+FoxP3^+/CD4^+$ time point 2	*P*				.082
	n/n_{miss}	10/0	4/0	6/0	
	Mean (SD)	0.14 (0.07)	0.09 (0.04)	0.17 (0.07)	
	95% CI	0.08–0.19	0.03–0.15	0.09–0.24	
	Median (IQR)	0.12 (0.12)	0.10 (0.06)	0.19 (0.10)	
	Minimum–maximum	0.04–0.24	0.04–0.12	0.05–0.24	
$CD8^+PD1^+/CD8^+$ baseline	*P*				.224
	n/n_{miss}	9/1	4/0	5/1	
	Mean (SD)	0.14 (0.10)	0.10 (0.09)	0.18 (0.10)	
	95% CI	0.07–0.22	−0.04 to 0.23	0.06–0.31	
	Median (IQR)	0.13 (0.18)	0.07 (0.12)	0.23 (0.10)	
	Minimum–maximum	0.03–0.29	0.03–0.22	0.03–0.29	
$CD8^+PD1^+/CD8^+$ time point 2	*P*				<.001
	n/n_{miss}	10/0	4/0	6/0	
	Mean (SD)	0.20 (0.13)	0.05 (0.03)	0.29 (0.07)	
	95% CI	0.10–0.29	−0.00 to 0.11	0.22–0.36	
	Median (IQR)	0.22 (0.27)	0.04 (0.04)	0.31 (0.07)	
	Minimum–maximum	0.03–0.36	0.03–0.11	0.17–0.36	
$CD4^+/CD8^+$ baseline	*P*				.088
	n/n_{miss}	9/1	4/0	5/1	
	Mean (SD)	1.20 (0.43)	0.93 (0.25)	1.41 (0.44)	
	95% CI	0.87–1.53	0.53–1.32	0.87–1.96	
	Median (IQR)	1.03 (0.33)	0.94 (0.33)	1.31 (0.83)	
	Minimum–maximum	0.60–1.88	0.60–1.21	0.98–1.88	
$CD4^+/CD8^+$ time point 2	*P*				.476
	n/n_{miss}	10/0	4/0	6/0	
	Mean (SD)	1.65 (0.99)	1.35 (1.22)	1.84 (0.86)	
	95% CI	0.94–2.35	−0.59 to 3.29	0.94–2.75	
	Median (IQR)	1.43 (1.76)	1.04 (1.65)	1.75 (1.29)	
	Minimum–maximum	0.27–3.07	0.27–3.07	0.68–3.05	
$CD4FoxP3^+/CD8^+$ baseline	*P*				**.020**
	n/n_{miss}	9/1	4/0	5/1	
	Mean (SD)	0.18 (0.09)	0.10 (0.07)	0.24 (0.03)	
	95% CI	0.11–0.24	−0.01 to 0.20	0.20–0.27	
	Median (IQR)	0.21 (0.17)	0.07 (0.07)	0.24 (0.03)	
	Minimum–maximum	0.06–0.28	0.06–0.20	0.21–0.28	
$CD4^+FoxP3^+/CD8^+$ time point 2	*P*				**.043**
	n/n_{miss}	10/0	4/0	6/0	
	Mean (SD)	0.21 (0.19)	0.09 (0.06)	0.30 (0.20)	
	95% CI	0.08–0.35	0.00–0.18	0.09–0.51	
	Median (IQR)	0.14 (0.19)	0.09 (0.09)	0.24 (0.28)	
	Minimum–maximum	0.03–0.63	0.03–0.16	0.12–0.63	

CI = confidence interval; IQR = interquartile range.
Bold indicates statistical significance.

Dose-Response Relationship and Dose-Immune Response Relationship

Mean and median doses applied to tumor were 127 and 120 Gy, respectively (100–234 Gy). Activity applied was 1,354 and 1,396 MBq, respectively (662–1,684 MBq). Mean tumor dose in responders was 116 Gy (100–144 Gy), and mean dose in nonresponders was 134 Gy (103–234 Gy; $P = .50$). A correlation was not found between tumor dose

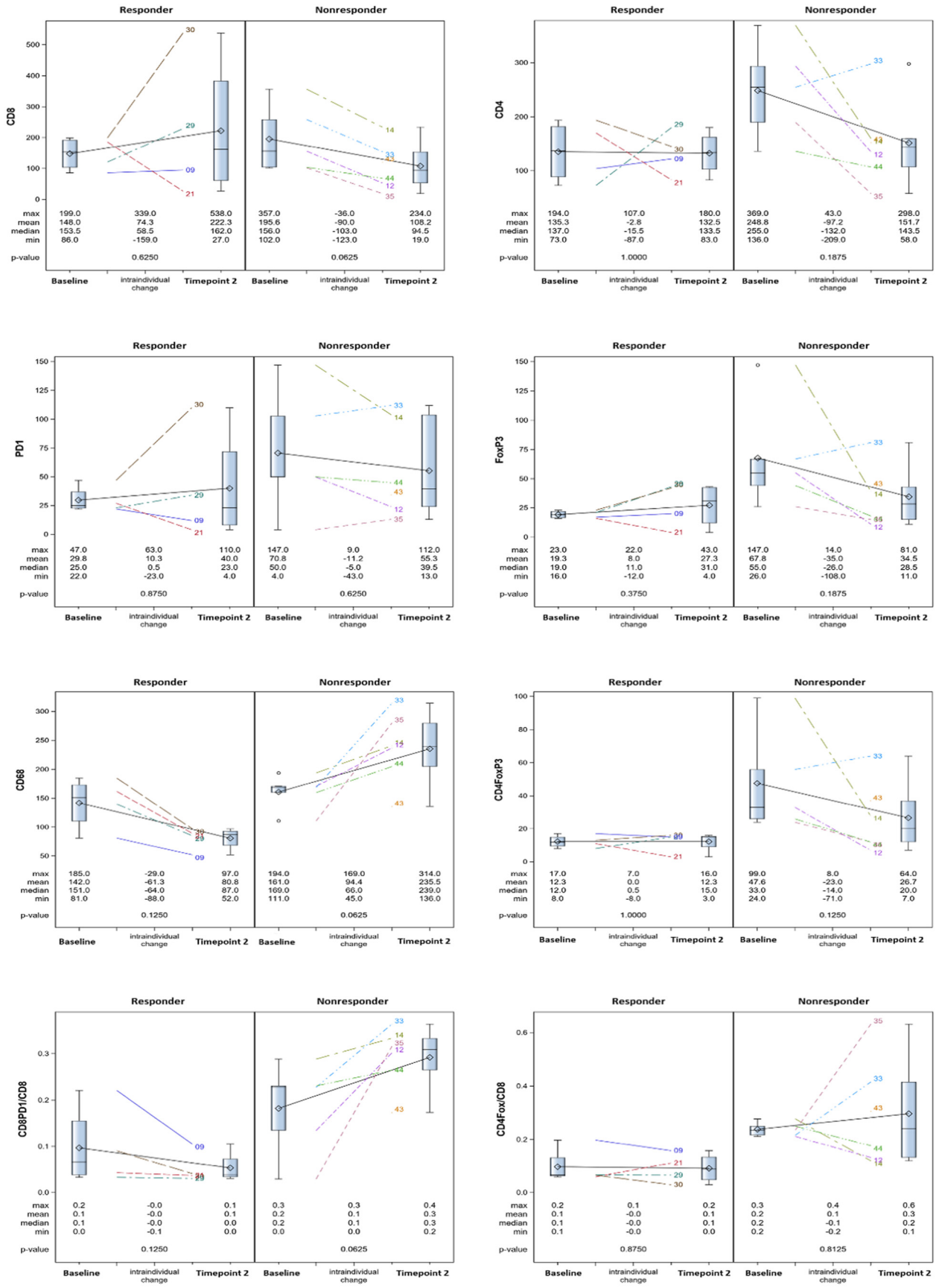

Figure 3. Subacute changes of immune cell infiltration after yttrium-90 transarterial radioembolization and their association with therapy response.

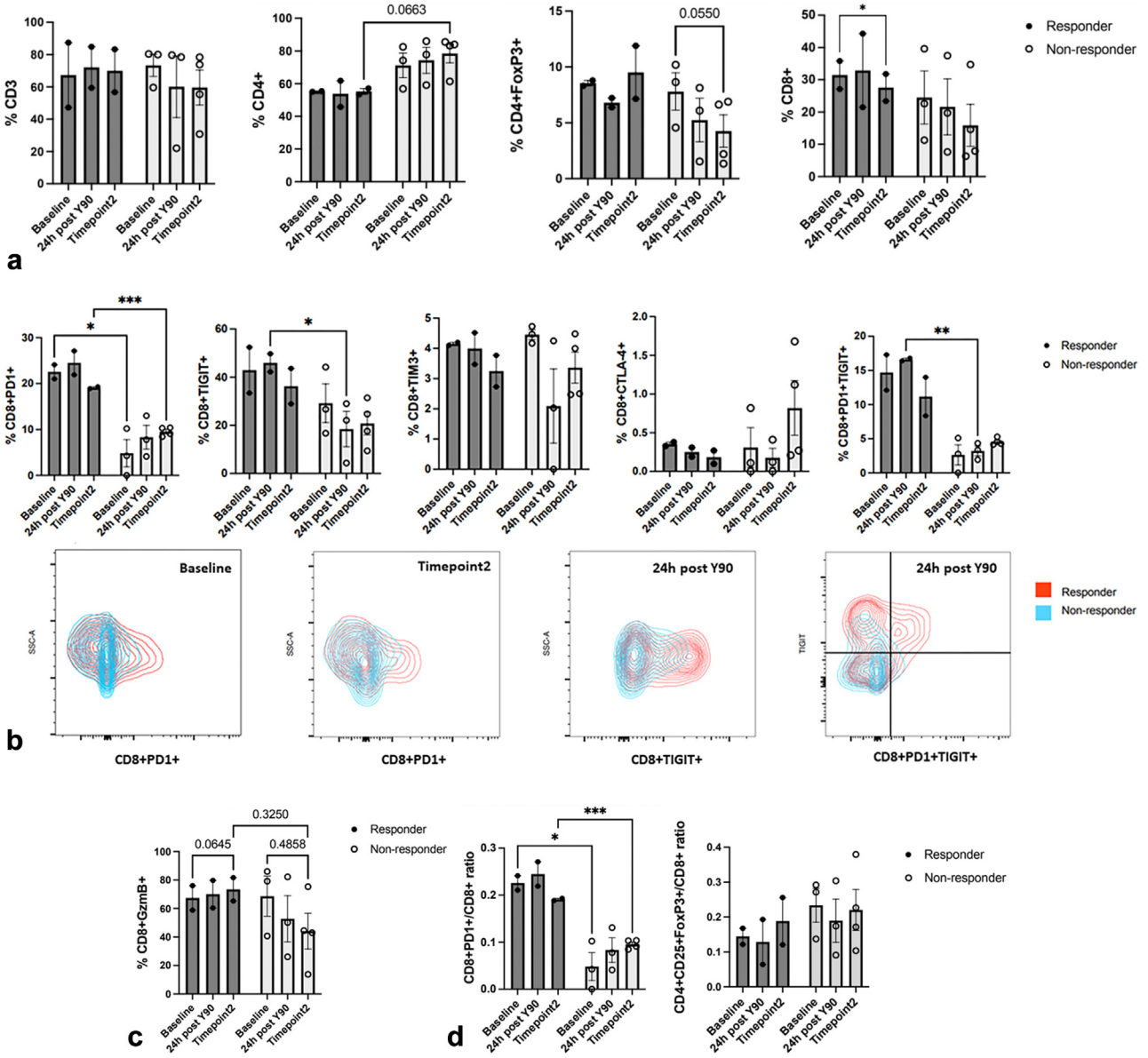

Figure 4. Peripheral immune cell development at baseline, 24 hours after yttrium-90 transarterial radioembolization, and time point 2 depicted by flow cytometry of peripheral blood mononuclear cells. **(a)** $CD3^+$, $CD4^+$; $CD4^+CD25^+FoxP3^+$, $CD8^+$ T cells; **(b)** $CD8^+PD1^+$, $CD8^+TIGIT^+$, $CD8^+TIM3^+$, $CD8^+CTLA4^+$, and $CD8^+PD1^+TIGIT^+$ T cells; **(c)** $CD8^+GzmB^+$; **(d)** $CD8^+PD1^+/CD8^+$ ratio and $CD4^+CD25^+FoxP3^+/CD8^+$ ratio.

and immune infiltration in distant tumor tissue ($CD4^+$ cells, $P = .869$; $CD8^+$ cells, $P = .512$; $FoxP3^+$ cells, $P = .753$; $CD68^+$ macrophages, $P = .612$; and $CD8^+PD1^+/CD8^+$ ratio, $P = .926$)

DISCUSSION

In this study, treatment of MSS colorectal liver metastases by ^{90}Y-TARE induced immunogenic effects in distant, untreated liver metastases. In CRC, immune infiltrates of the tumor microenvironment impact tumor cell death, and cytotoxic T cells are positively associated with increased cytolitic activites and prolonged survival (13,14). A recent study suggested that $FoxP3^+$ Treg density evaluation in tumor tissue and normal colorectal tissue positively correlate vascular and perineural invasions, which increased the prognostic accuracy of patients with CRC (15). Furthermore, $CD8^+$ $PD1^+$ T cells exhibit an exhausted phenotype as defined by an impairment of proliferation, cytokine production, and cytotoxicity. Additionally, tumor associated macrophages positively correlate with tumor growth through multiple signaling pathways, with tumor cells also making use of tumor associated macrophages to support tumor progression (16–19). Emerging evidence suggests that immune cell properties may be superior to the TNM stage as a prognosticator in CRC (20).

In the study described herein, a multiplex immunofluorescent staining panel comprising 5 immune cell markers were used to quantify and characterize tumor infiltration of lymphocytes in liver metastases before and after contralateral ^{90}Y-TARE. Patients were stratified as responders and nonresponders based on tumor control or progression during follow-up. Before therapy, responders displayed lower concentrations of FoxP3$^+$ cells and colocation of CD4$^+$FoxP3$^+$ cells compared with nonresponders. After receiving unilobar ^{90}Y-TARE, untreated liver metastases of nonresponders showed an increase in CD68$^+$ macrophages density at time point 2. Compared with nonresponders, responders displayed less CD4$^+$FoxP3$^+$ regulatory T cells than CD8$^+$ T cells in the same ROI at both time points. Nonresponders demonstrated a trend of increasing CD68$^+$ macrophages at time point 2 compared with baseline. In addition, nonresponders had a higher CD8$^+$PD1$^+$/CD8$^+$ ratio in tumor tissue.

Flow cytometry of PBMC was additionally performed to confirm tissue findings by demonstrating systemic effects in blood. Nonresponders showed a lower percentage of circulating CD8$^+$PD1$^+$ T cells and a lower CD8$^+$PD1$^+$/CD8$^+$ ratio both at baseline and time point 2. Thus, reversed immune effects were confirmed of the same T cell type on a tissue level and systemically. It was hypothesized that these results reflect phenotypic changes of CD8$^+$ T cells as an effect of recirculation and peripheral exhaustion. This reversed tissue and systemic effect has also been shown by previous studies (21–23). In nonresponders, ^{90}Y-TARE might induce clonal expansion of exhausted CD8$^+$ T cells with consecutive enrichment in distant untreated lesions. The intratumoral recruitment of exhausted T cells leading to cancer progression and the consecutive derichment in the circulation of nonresponders might be potentiated by the release of chemokines, an effect frequently observed after ^{90}Y-TARE (24). In this cohort, the circulating fraction of CD8$^+$ T cells coexpressed PD1 and TIGIT (known to inhibit innate and adaptive immunity), and the posttherapy percentage of this cell subpopulation was lower in nonresponders compared with responders. In melanoma, simultaneous TIGIT and PD1 blockade increases cytokine production and cytotoxic activity of CD8$^+$ T cells (25).

Most patients with CRC do not benefit from checkpoint inhibitors due to the immunosuppressive tumor microenvironment of MSS tumors predominant in CRC (26–28). In a previous trial of intrahepatic metastatic CRC, Wang et al (6) combined ^{90}Y-TARE with PD1 and CTLA4 blockade. All patients displayed tumor progression. Seven patients underwent biopsy in ^{90}Y-exposed lesions before and after radioembolization plus checkpoint inhibitor treatment. All patients showed no change in a low proportion of tumor infiltrating immune cells (CD8$^+$, CD68$^+$, CD4$^+$ T cells) in irradiated tumors (6).

Even though Wang et al (6) did not show immunogenic response in their cohort, their results were contradictory to those of this study. As in this cohort, all patients were MSS. However, in contrast to the study by Wang et al (6), this analyses comprised distant, untreated liver lesions—in contrast to irradiated and consecutively resected lesions in the referenced study. In addition, immunogenic tissue effects in this study were supported by systemic immune response in peripheral circulating cells.

Effects observed in this study may have prognostic value, such as increased CD68 or an increase of CD8$^+$PD1$^+$/CD8$^+$ ratio, or low baseline FoxP3$^+$ regulatory cells and colocation of CD4$^+$FoxP3$^+$ cells. Additionally, ^{90}Y-TARE modified PD1 expression in tissue of nonresponders. These patients displayed an increased CD8$^+$PD1$^+$/CD8$^+$ ratio with an unchanged relative number of CD8$^+$ positive T cells. Therefore, it was hypothesized that in nonresponders PD1 checkpoint blockade may offer benefit. As described by Kumagai et al (29), the PD1 expression balance between effector and regulatory T cells predicts the clinical effectiveness of PD1 blockade therapies, and PD1 expression by CD8$^+$ T cells negatively impacts effector and immunosuppressive functions, respectively. PD1 blockade also induces recovery of dysfunctional PD1$^+$CD8$^+$ T-cell immunosuppression. Moreover, reactivation of effector PD1$^+$CD8$^+$ T cells by PD1 blockade induced clinical tumor regression (29).

Limitations of this study must be acknowledged. This cohort was small, and findings must be validated in larger patient groups. There was an imbalance of sex distribution, with only 1 woman. Immunogenic effects may vary according to sex (12). Multiplex immunophenotyping analyses were conducted using core needle biopsies instead of larger resection material with the risk of sampling bias. Half of the patients underwent biopsy of identical tumors at 2 time points. However, flow cytometry of PBMCs supported outcomes of tissue analyses by demonstrating systemic immunogenic effects. Time points for tissue biopsy after ^{90}Y-TARE varied. A recent study by Pinato et al (30) on resected HCC specimen after transarterial chemoembolization demonstrated a correlation of immunogenic changes with overall survival. In this study, sample acquisition ranged from 2 to 11 months (median, 3.4 months). Variability of time points did not harm signal identification in their cohort (30). Similarly, despite varying time points for tissue acquisition, this study successfully demonstrated discrimination between responders and nonresponders based on immunogenic effects both locally and systemically.

In summary, ^{90}Y-TARE led to immunogenic modulation of the tumor microenvironment in distant tumors, as well as systemic immunogenic responses. The majority of patients with CRC currently do not benefit from checkpoint inhibitors in predominant MSS tumors. Yet, based on this study, potential mechanisms of interaction were noted, in specific increases of CD8$^+$PD1$^+$/CD8$^+$ ratio in nonresponders. Further studies are warranted to elucidate the prognostic significance of immune cell subsets as well as synergism of ^{90}Y-TARE and checkpoint inhibition in MSS CRC.

ACKNOWLEDGMENTS

Funding for laboratory analyses was provided by Sirtex Medical, Woburn, Massachusetts. The authors wish to thank the Department of Radiology's Study Center for study management, Regina Schinner for support with statistical analysis, and all patients for taking part in the study.

AUTHOR INFORMATION

From the Department of Radiology (E.Ö., M.A.-F., L.S., M.M.R.S., L.F.B., H.H.-E., M.A.K., M.S., M.W., J.R.), Center of Integrated Protein Science Munich (CIPS-M) and Division of Clinical Pharmacology, Department of Medicine IV (I.P., M.T.), Department of Medicine II (I.P.), Department of Nuclear Medicine (M.J.Z.), and Department of Pathology (M.R.), LMU University Hospital, LMU Munich, Germany; and Goldyne Savad Institute of Gene Therapy and Division of Image-guided Therapy and Interventional Oncology (S.N.G.), Department of Radiology, Hadassah Hebrew University Medical Center, Jerusalem, Israel. Received January 25, 2024; final revision received July 5, 2024; accepted July 14, 2024. Address correspondence to J. R., Department of Radiology, University Hospital, LMU Munich, Marchioninistr 15, 81377 Munich, Germany; E-mail: Jens.Ricke@med.uni-muenchen.de; Twitter handle: @LMU_Radiology

M.J.Z. reports consulting fees from Boston Scientific and honoraria from Sirtex Medical Europe and Terumo. M.S. is supported by AstraZeneca, Roche, Bayer, and Sirtex Medical and receives proctor fees from Sirtex Medical. M.W. receives proctor fees from Sirtex Medical. S.N.G. receives funding from the Israel Science Foundation and consulting fees from Cosman Medical and XACT robotics. J.R. is supported by Sirtex Medical and reports laboratory materials and honoraria from Sirtex Medical.

REFERENCES

1. Sung H, Ferlay J, Siegel RL, et al. Global cancer statistics 2020: GLOBOCAN estimates of incidence and mortality worldwide for 36 cancers in 185 countries. CA Cancer J Clin 2021; 71:209–249.
2. André T, Shiu KK, Kim TW, et al. Pembrolizumab in microsatellite-instability-high advanced colorectal cancer. N Engl J Med 2020; 383: 2207–2218.
3. Arnold CN, Goel A, Compton C, et al. Evaluation of microsatellite instability, hMLH1 expression and hMLH1 promoter hypermethylation in defining the MSI phenotype of colorectal cancer. Cancer Biol Ther 2004; 3:73–78.
4. Cervantes A, Adam R, Roselló S, et al. Metastatic colorectal cancer: ESMO Clinical Practice Guideline for diagnosis, treatment and follow-up. Ann Oncol 2023; 34:10–32.
5. Chew V, Lee YH, Pan L, et al. Immune activation underlies a sustained clinical response to yttrium-90 radioembolisation in hepatocellular carcinoma. Gut 2019; 68:335–346.
6. Wang C, Park J, Ouyang C, et al. A pilot feasibility study of yttrium-90 liver radioembolization followed by durvalumab and tremelimumab in patients with microsatellite stable colorectal cancer liver metastases. Oncologist 2020; 25:382-e776.
7. Ramdhani K, Smits MLJ, Lam M, Braat A. Combining selective internal radiation therapy with immunotherapy in treating hepatocellular carcinoma and hepatic colorectal metastases: a systematic review. Cancer Biother Radiopharm 2023; 38:216–224.
8. Powerski M, Drewes R, Omari J, Relja B, Surov A, Pech M. Intra-hepatic abscopal effect following radioembolization of hepatic metastases. Cardiovasc Intervent Radiol 2020; 43:1641–1649.
9. Seidensticker R, Seidensticker M, Damm R, et al. Hepatic toxicity after radioembolization of the liver using 90 Y-microspheres: sequential lobar versus whole liver approach. Cardiovasc Intervent Radiol 2012; 35: 1109–1118.
10. Sangro B, Martínez-Urbistondo D, Bester L, et al. Prevention and treatment of complications of selective internal radiation therapy: expert guidance and systematic review. Hepatology 2017; 66: 969–982.
11. van Hazel GA, Heinemann V, Sharma NK, et al. SIRFLOX: randomized phase III trial comparing first-line mFOLFOX6 (plus or minus bevacizumab) versus mFOLFOX6 (plus or minus bevacizumab) plus selective internal radiation therapy in patients with metastatic colorectal cancer. J Clin Oncol 2016; 34:1723–1731.
12. Heinrich K, Modest DP, Ricard I, et al. Gender-dependent survival benefit from first-line irinotecan in metastatic colorectal cancer. Subgroup analysis of a phase III trial (XELAVIRI-study, AIO-KRK-0110). Eur J Cancer 2021; 147:128–139.
13. Khan H, Pillarisetty VG, Katz SC. The prognostic value of liver tumor T cell infiltrates. J Surg Res 2014; 191:189–195.
14. Katz SC, Bamboat ZM, Maker AV, et al. Regulatory T cell infiltration predicts outcome following resection of colorectal cancer liver metastases. Ann Surg Oncol 2013; 20:946–955.
15. Suzuki H, Chikazawa N, Tasaka T, et al. Intratumoral CD8(+) T/FOXP3 (+) cell ratio is a predictive marker for survival in patients with colorectal cancer. Cancer Immunol Immunother 2010; 59:653–661.
16. Barbera-Guillem E, Nyhus JK, Wolford CC, Friece CR, Sampsel JW. Vascular endothelial growth factor secretion by tumor-infiltrating macrophages essentially supports tumor angiogenesis, and IgG immune complexes potentiate the process. Cancer Res 2002; 62: 7042–7049.
17. Liu Y, Cao X. The origin and function of tumor-associated macrophages. Cell Mol Immunol 2015; 12:1–4.
18. Qian BZ, Pollard JW. Macrophage diversity enhances tumor progression and metastasis. Cell 2010; 141:39–51.
19. Yang L, Zhang Y. Tumor-associated macrophages: from basic research to clinical application. J Hematol Oncol 2017; 10:58.
20. Galon J, Mlecnik B, Bindea G, et al. Towards the introduction of the 'Immunoscore' in the classification of malignant tumours. J Pathol 2014; 232:199–209.
21. Ma J, Zheng B, Goswami S, et al. PD1(Hi) CD8(+) T cells correlate with exhausted signature and poor clinical outcome in hepatocellular carcinoma. J Immunother Cancer 2019; 7:331.
22. Gough MJ, Crittenden MR. The paradox of radiation and T cells in tumors. Neoplasia 2022; 31:100808.
23. Blair TC, Alice AF, Zebertavage L, Crittenden MR, Gough MJ. The dynamic entropy of tumor immune infiltrates: the impact of recirculation, antigen-specific interactions, and retention on T cells in tumors. Front Oncol 2021; 11:653625.
24. Carpizo DR, Gensure RH, Yu X, et al. Pilot study of angiogenic response to yttrium-90 radioembolization with resin microspheres. J Vasc Interv Radiol 2014; 25:297–306.e1.
25. Simon S, Voillet V, Vignard V, et al. PD-1 and TIGIT coexpression identifies a circulating CD8 T cell subset predictive of response to anti-PD-1 therapy. J Immunother Cancer 2020; 8:e001631.
26. Modest DP, Pant S, Sartore-Bianchi A. Treatment sequencing in metastatic colorectal cancer. Eur J Cancer 2019; 109:70–83.
27. Arai H, Battaglin F, Wang J, et al. Molecular insight of regorafenib treatment for colorectal cancer. Cancer Treat Rev 2019; 81:101912.
28. Le DT, Uram JN, Wang H, et al. PD-1 blockade in tumors with mismatch-repair deficiency. N Engl J Med 2015; 372:2509–2520.
29. Kumagai S, Togashi Y, Kamada T, et al. The PD-1 expression balance between effector and regulatory T cells predicts the clinical efficacy of PD-1 blockade therapies. Nat Immunol 2020; 21: 1346–1358.
30. Pinato DJ, Murray SM, Forner A, et al. Trans-arterial chemoembolization as a loco-regional inducer of immunogenic cell death in hepatocellular carcinoma: implications for immunotherapy. J Immunother Cancer 2021; 9:e003311.

APPENDIX A

Multiplex Immunophenotyping

Immunofluorescence staining of paraffin sections was performed using the Opal 7 Solid Tumor Immunology Kit (Akoya Biosciences, Marlborough, Massachusetts), according to the recommended protocol. Briefly, 2-μm–thick tissue sections were cut from formalin-fixed, paraffin-embedded tissues and heated in a dry oven at 58°C for 2 hours, washed with xylene, and hydrated through an ethanol gradient ending with a distilled water wash. After fixation with neutral-buffered formalin, antigen retrieval was performed in boiling AR6 (pH 6) or AR9 (pH 9) buffer, followed by blocking (10 minutes in ARD1001EA) and primary antibody incubation (30 minutes at room temperature). Anti-CD4, anti-CD8, anti-FoxP3, anti-CD68, and anti-PanCK primary antibodies were part of the kit. In addition, anti-PD1 (clone EPR4877, dilution 1/150; Abcam, Cambridge, United Kingdom) was used. Secondary antibody incubation (10 minutes at room temperature) was performed in the Opal Polymer HRP ARH1001EA secondary antibody solution, followed by incubation with Opal fluorophores (Opal 520, Opal 540, Opal 570, Opal 620, Opal 650, and Opal 690; 10 minutes at room temperature). After each staining cycle, antibody removal was performed using AR buffers. Slides were counterstained with DAPI FP1490A (Akoya Biosciences) for 5 minutes and mounted in Vectrashield Plus Antifade Mounting Medium H-2000 (Vector Laboratories, Burlingame, California). Image acquisition was obtained using the VectraPolaris scanning system (Akoya Biosciences). Slides were scanned at 10× magnification in order to select the region of interest. Second scanning was performed at high-powered imaging (20× magnification; resolution of 0.5 μm per pixel; 0.682 μm × 0.510 μm) using Phenochart (Akoya Biosciences). Image analysis was performed using the ImageJ software (1). For cell quantification, the most representative intratumoral areas were chosen by a board-certified pathologist (E.Ö.) blinded to clinical information. Tumor cells were defined as PanCK-positive cells displaying a malignant morphology. Necrotic areas were confirmed by hematoxylin–eosin staining. For each tissue sample collected at baseline and time point 2, the amount of infiltrating immune cells in the intratumoral regions of the lesions and the phenotypic characteristics of each cell type were evaluated.

SUPPLEMENTAL REFERENCE

1. Rasband WS. National Institutes of Health. 2011. Available at: http://imagej.nih.gov/ij/. Accessed June 16, 2023.

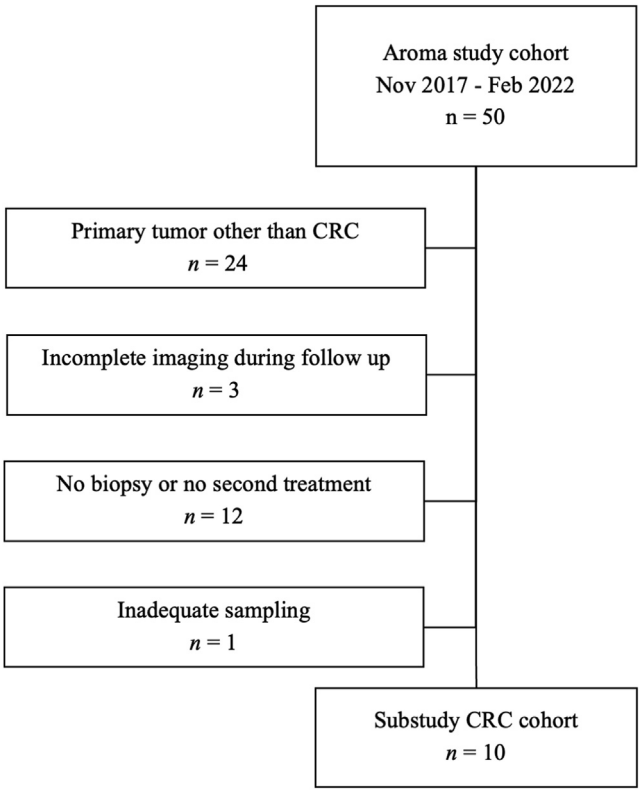

Figure E1. Flow chart showing the distribution of liver cancer patients with respect to patient inclusion/exclusion. CRC = colorectal cancer.

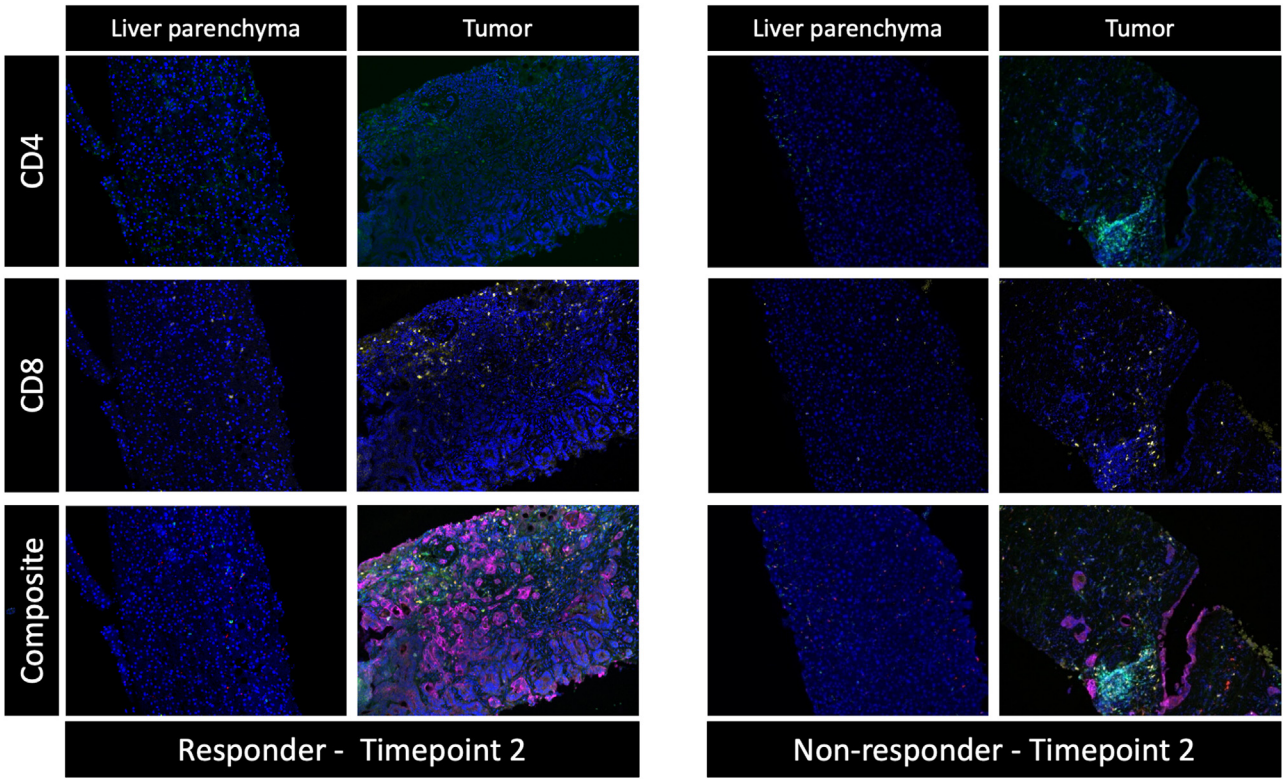

Figure E2. Representative images of CD4, CD8, and composite CD4, CD8, CD68, FoxP3, PD1, and PanCK multiplex immunofluorescence staining in nontumoral liver tissue compared with the tumor tissue in responder and nonresponder patients at time point 2. Note the difference between infiltration pattern in tumor microenvironment and normal liver.

Table E1. Treatment Characteristics of Patients Before and After Radioembolization and During Follow-up

Treatment characteristic	Before radioembolization*	During follow-up
Liver resection	5/10	1/10
Local ablation	0/10	0/10
Systemic treatment		
First line		
Fluorouracil	1/10	2/10
Oxaliplatin based	5/10	0/10
Irinotecan based	3/10	1/10
Second line		
Fluorouracil	1/10	1/10
Oxaliplatin based	1/10	0/10
Irinotecan based	5/10	0/10
Bevacizumab	8/10	2/10
Other therapies†	5/10	—

*Washout time of systemic treatments was always >21 days, liver resection >1 years.
†Panitimumab, bbi-608, aflibercept, and cetuximab.

Table E2. The Function of İmmune Cells and Cell Surface Markers in the Liver İmmune Microenvironment of CRLM.

Cell surface marker	Cell type	Function	Protumor/antitumor function
$CD3^+CD4^+$	T helper	Regulation of immune response by the production and release of cytokines such as IFNγ and TNFα	Mainly antitumorogenic
$CD4^+CD25^+FoxP3^+$	Regulatory T cell	Maintenance of self-tolerance; in cancer, suppression of the activation and proliferation of effector T cells	Protumorogenic
$CD3^+CD8^+$	Effector T cell	Secretion of cytokines (mainly TNFα and INFγ), induction of apoptosis through the Fas/FasL pathway, secretion of cytotoxic granules	Antitumorogenic
$CD3^+CD8^+GzmB^+$	Cytotoxic T cell	Induction of apoptosis through the release of perforin and granzymes, through the binding of corresponding antigens on target cells	Antitumorogenic
$CD68^+$	Macrophage	Presentation of exogenous antigens to T cells through MHC-I and MHC-II, regulation of T-cell activation	M1 Antitumoogenic; M2 Protumorogenic

CRLM = colorectal liver metastasis; IFN = interferon; MHC = major histocompatibility complex; TNF = tumor necrosis factor.

Table E3. The Change Rate of Immune Cells (Ratio between Time Point 2 and Baseline for Nonresponder Patients)

Patient number	CD8 baseline	CD8 time point 2	CD8 time point2/baseline	*P*
Nonresponder 1	259	154	0.59	
Nonresponder 2	102	19	0.18	
Nonresponder 3	ND	121	ND	
Nonresponder 4	104	68	0.65	
Nonresponder 5	156	53	0.34	
Nonresponder 6	357	234	0.65	
Mean value (SD)	195.60 (110.44)	108.17 (78.37)	–90 (33.35)	.062
Patient number	**CD68 baseline**	**CD68 time point 2**	**CD68 time point 2/baseline**	
Nonresponder 1	169	314	1.86	
Nonresponder 2	111	280	2.52	
Nonresponder 3	ND	136	ND	
Nonresponder 4	160	205	1.28	
Nonresponder 5	171	237	1.39	
Nonresponder 6	194	241	1.24	
Mean value (SD)	161.00 (30.63)	235.50 (61.65)	94.40 (58.35)	.062
Patient number	**CD8PD1/CD8 baseline**	**CD8PD1/CD8 time point 2**	**CD8PD1/CD8 time point 2/ CD8PD1/CD8 baseline**	
Nonresponder 1	0.23	0.36	1.60	
Nonresponder 2	0.029	0.32	10.73	
Nonresponder 3	ND	0.17	ND	
Nonresponder 4	0.23	0.26	1.14	
Nonresponder 5	0.13	0.30	2,24	
Nonresponder 6	0.29	0.33	1.16	
Mean value (SD)	0.18 (0.10)	0.29 (0.07)	0.13 (0.10)	.062

ND = not detected.

Table E4. T-Cell Coinhibitory Receptors, Ligands, and Signaling Pathways

Immune checkpoint receptors	Cellular expression	Ligand	Signaling pathways
CTLA-4	T cells	CD80, CD86	SHP2, LCK/ZAP70/PI3K, PP2A/AKT
PD1	T cells, B cells, NKT cells, monocytes	PD-L1, PD-L2	SHP1, PI3K/AKT SHP2, LCK/ZAP70/PI3K, RAS
TIGIT	T cells, NK cells, NKT cells	CD155, CD112	NF-kB, PI3K, MAPK
TIM-3	T cells, B cells, NK cells, NKT cells, DCs, macrophages	Gal-9	PI3K, BAT3/LCK

CTLA = cytotoxic T-lymphocyte–associated protein; PD = programmed cell death; TIGIT = T-cell immunoreceptor with immunoglobulin and ITIM domains; TIM = T-cell immunoglobulin and mucin-containing protein 3 (1).